Proceedings of the Canadian Society for Mechanical Engineering International Congress
32nd Annual Conference of the Computational Fluid Dynamics Society of Canada
Canadian Society of Rheology Symposium
CSME-CFDSC-CSR 2025
May 25–28, 2025, Montréal, Québec, Canada

Experimental Verification of a Local Thermal Non-Equilibrium Model for a Horizontal Cylindrical Magnetite-Based Rock Bed as a Thermal Battery

Seyed Soheil Mousavi Ajarostaghi*, Leyla Amiri, Sébastien Poncet
Mechanical Engineering Department, Université de Sherbrooke, Sherbrooke, Canada
*e-mail address: seyed.Soheil.Mousavi.Ajarostaghi@USherbrooke.ca

Abstract—Researchers have recently utilized and examined rock beds as one of the viable choices for sensible heat storage methods. This system's primary benefits are its inexpensive cost and the availability of rock used in the bed to store thermal energy. During the charging process, the heat transfer fluid passes through the pores of the rock bed, storing heat in the bed's solid matrix. The bed's porous structure allows fluids, whether compressible or incompressible, to pass through it, retaining heat in the solid portion of the porous area. In the discharging process, the fluid, on the other hand, takes the stored heat on demand. Researchers have been working diligently to study fluid flow and heat transfer in the porous structure of rock beds, as these areas are complex due to their heterogeneous nature in real-world applications. Although heat transport in rock beds has been extensively studied experimentally and modeled numerically, there is no support for Local Thermal Non-Equilibrium (LTNE)-based thermal models, particularly for horizontal cylindrical magnetite rock beds. There is a knowledge gap regarding the dynamics of heat retention in rock beds with air flow and under low-temperature conditions, as most research focuses on packed bed systems with water-based fluids and high-temperature conditions. This work bridges this gap by experimentally examining the heat storage and discharge dynamics in a cylindrical, horizontally aligned magnetite rock bed. The acceptable accuracy of the developed model is demonstrated by the numerical results derived from the proposed LTNE model. The experimental and numerical outcomes exhibit a maximum error of 6%.

Keywords; Thermal Energy Storage (TES), Sensible Heat Storage, Local Thermal Non-Equilibrium (LTNE), Magnetite-Based Rock Bed, Numerical Modeling

I. INTRODUCTION

Thermal management and waste heat storage are two significant challenges facing many enterprises today, particularly those that rely on renewable energy sources. The two main approaches for thermal energy storage (TES) systems are (i) sensible and (ii) latent, each of which has unique benefits and drawbacks [1]. Unlike sensible energy storage systems, latent heat energy storage systems may store a substantial quantity of energy in a given period due to the phase change process; nevertheless, these systems have high initial and ongoing costs and require precise control systems. Sensible TES systems, however, require more area to provide the same energy as latent systems because they contain less stored energy. A larger mass of the desired substance is required to store the same amount of energy. Since there is no phase change process, sensible TES systems have a simpler control system, allowing them to be installed in environmental dead space to address the space problem [2].

As an efficient sensible TES system, rock beds have lately garnered considerable interest as a viable solution for a heat storage system. Its primary benefits are the availability of rock utilized in the bed to store thermal energy and the system's affordability. The rock bed's porous structure allows fluid movement, whether compressible or incompressible, to pass through, storing heat within the solid portion of the porous area. This process is called charging. On the other hand, the stored heat can be released by discharging the system when energy demand arises [3]. Rock beds have gained popularity as an effective and low-cost alternative for sensible TES due to their high heat capacity, thermal stability, and extended lifespan [4]. Unlike phase change materials (PCMs) or chemical heat storage systems, rock beds use sensible heat storage, which absorbs and releases thermal energy through a solid medium without a phase shift [5].

Scalability and material availability are two key benefits of rock beds that make them suitable for various energy storage applications, including waste heat recovery, solar energy storage, and heating systems [6]. However, because voids affect fluid dynamics and thermal performance, increasing the thermal efficiency of rock beds necessitates a thorough understanding of heat transfer processes inside porous media [7].

In porous rock beds, convection governs fluid-solid heat exchange, whereas conduction predominates within the solid matrix. The solid's and the working fluid's thermal

characteristics, flow rate, porosity, and particle size all affect how well heat is transferred [7].

Because non-uniform pore structures result in pressure losses and variable heat transfer rates, the flow of porous media in rock beds is extremely complex [7]. To estimate flow resistance in porous structures, researchers frequently use the Forchheimer extension and Darcy's Law [8]. Since the temperature differential between the fluid and solid phases can be substantial, especially at large heat fluxes, the Local Thermal Equilibrium (LTE) assumption is frequently incorrect in thermal modeling. By considering solid and fluid temperatures independently, the Local Thermal Non-Equilibrium (LTNE) model provides a more accurate method, enhancing predictions for high-temperature applications and packed beds [9]. The accuracy of LTNE models in capturing thermal gradients and transient heat transport behaviors in rock beds, particularly when fluid flow conditions alter, is confirmed by previous research [10]. However, there remains a lack of additional experimental confirmation, particularly for rock beds based on magnetite.

The objective of this study is to experimentally verify the LTNE numerical model for heat transfer analysis in a magnetite-based rock bed thermal battery using Computational Fluid Dynamics (CFD). To better understand how heat is stored in the solid phase and transferred to the fluid phase, the study examines the charging and discharging processes (two 4-hour cycles of charging (2 hours) and discharging (2 hours) consecutively, a total of 8 hours of testing and simulation) through controlled experiments conducted in a horizontal cylindrical rock bed. To evaluate how well LTNE modeling predicts temperature distributions and heat transfer dynamics in porous media, the experimental data are then contrasted with CFD simulations. The validated LTNE numerical model can then be employed to examine the impact of various factors on thermal performance, with the goal of enhancing the efficiency and design of rock bed TES systems.

II. Methodology

A. Experimental Setup

Figures 1a and 1b illustrate the schematic of the experimental setup, including equipment details and geometric factors. Additionally, the experimental setup picture is illustrated in Figure 1c. Table I contains the values for the experimental setup's geometrical and operational features. The used temperature sensors are stainless steel K-type thermocouples. According to the manufacturer details, their accuracy is ±2.2°C. The employed heat gun is a 5400-Watt type with an accuracy of ±1% (manufacturer report).

The rock type employed in the proposed rock bed here is magnetite. This material was presented as the optimum choice for high-temperature TES systems with rock beds as a sensible thermal energy storage system [13]. One of the primary iron ores, magnetite, is a mineral with the chemical formula $Fe^{2+}Fe^{3+}{}_2O_4$. It is ferrimagnetic and one of the iron oxides. It can be magnetized to become a permanent magnet, as it is attracted to magnets. Of all the naturally occurring minerals on Earth, it is the most magnetic, except for incredibly rare native iron deposits. Magnetite has a Mohs hardness of 5–6 and leaves a black streak. It is black or brownish-black with a metallic sheen. Both igneous and metamorphic rocks contain small magnetite granules [12].

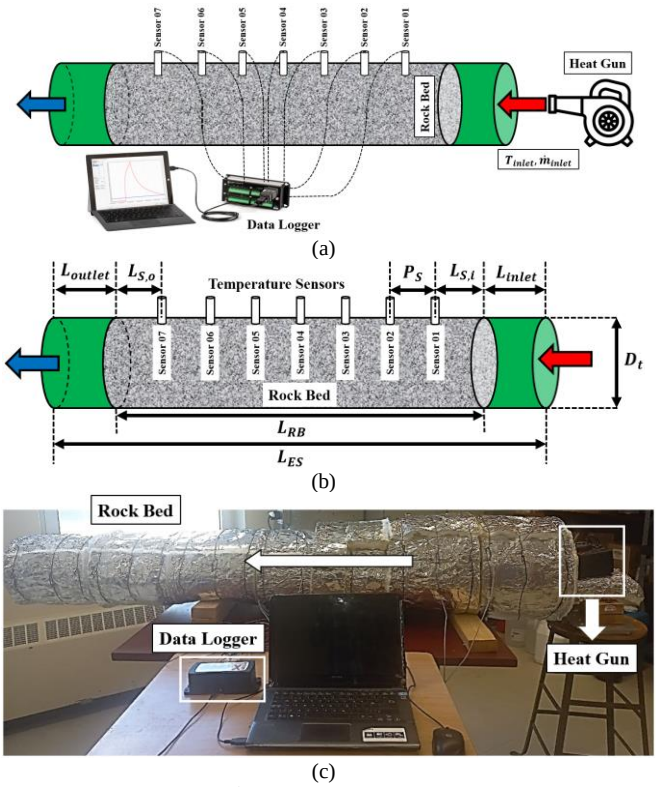

Figure 1. (a) Schematic of the experimental setup with equipment details, (b) schematic of the experimental setup with geometric factors, and (c) picture of the experimental setup [11]

TABLE I. The Experimental Setup's Geometrical and Operational Factor Characteristics

Property	Symbol	Value
Diameter of the tube [mm]	D_t	101.6
Length of the rock bed [mm]	L_{RB}	1730
Length of the experimental setup [mm]	L_{ES}	2000
Distance between the sensors [mm]	P_S	200
Thickness of the pipe [mm]	th_P	3
Maximum thickness of insulation [mm] (from inlet to a distance of 870 mm)	$thi_{,Max}$	160
Minimum thickness of insulation [mm]	$thi_{,Min}$	120
Length of the inlet part [mm]	L_{inlet}	160
Length of the outlet part [mm]	L_{outlet}	110
Distance from the first sensor to the beginning of the rock bed [mm]	$L_{S,i}$	100
Distance from the last sensor to the end of the rock bed [mm]	$L_{S,o}$	100
Inlet flow velocity [m.s^{-1}]	V_{Inlet}	2.2
Rock bed porosity [-]	ε	0.37
Average diameter of rocks [mm]	d_P	8
Inlet temperature in charge mode [°C]	$T_{inlet,\ Charge}$	70
Inlet temperature in discharge mode [°C]	$T_{inlet,\ Discharge}$	31
Initial temperature [°C]	$T_{initial}$	23

B. Numerical Model

Considering the incompressibility of the airflow, the continuity equation (mass conservation) may be written as:

$$\nabla . \boldsymbol{u} = 0 \quad (1)$$

where $\boldsymbol{u}$ is the velocity vector.

The momentum equation is altered to incorporate Darcy and Forchheimer resistance terms when a porous medium is present [7,9]:

$$\rho \frac{D\boldsymbol{u}}{Dt} = -\nabla P + \mu . \nabla^2 \boldsymbol{u} - \left(\frac{\mu}{K}\boldsymbol{u} + C_{inertial} . \rho |\boldsymbol{u}| \boldsymbol{u}\right) \quad (2)$$

where ρ, P, μ, K, and $C_{inertial}$ are fluid density, pressure, dynamic viscosity, permeability, and Forchheimer coefficient (inertial loss), respectively.

For modeling the turbulent flow, the *k-ω SST* model was employed. The *k-ω SST* model consists of two transport equations for (i) the turbulence kinetic energy (k) and (ii) the specific dissipation rate (ω), as follows:

Turbulence Kinetic Energy Equation (k-equation):

$$\frac{\partial k}{\partial t} + \boldsymbol{u}.\nabla k = P_k - \beta^* k\omega + \nabla.\left[\left(\nu + \frac{\nu_t}{\sigma_k}\right)\nabla k\right] \quad (3)$$

Specific Dissipation Rate Equation (ω-equation):

$$\frac{\partial \omega}{\partial t} + \boldsymbol{u}.\nabla \omega = \frac{\gamma}{\nu_t}P_k - \beta\omega^2 + \nabla.\left[\left(\nu + \frac{\nu_t}{\sigma_\omega}\right)\nabla\omega\right] + 2(1-F_1)\frac{\sigma_\omega}{\omega}\nabla k.\nabla\omega \quad (4)$$

where P_k, ν_t, F_1, and γ are the production of turbulence kinetic energy, turbulent eddy viscosity, blending function for near-wall effects, and the rate at which turbulence kinetic energy is converted into dissipation. σ_k and σ_ω are the turbulent Prandtl numbers for k and ω, respectively. β and β* are the empirical model constants.

The commercial CFD, ANSYS Fluent 2023 R2, based on the finite volume method, was used for all calculations. Viscous and inertial resistances should be set as the inputs for modeling the porous media, which can be calculated using the Ergun equation. This model is a quasi-empirical relationship that relates the pressure drop along a porous bed to the apparent velocity. This model is widely used for visualizing flow in porous materials and modeling their physical properties. The equation inputs are fluid properties and bed properties. A form of the equation corrects the friction factor with the Reynolds number. While Darcy and Blake-Kozeny-Carman (BKC) models include only viscous terms, the Ergun model incorporates both viscous and inertial terms [9]:

$$\frac{|\Delta p|}{L} = \frac{150\mu(1-\varepsilon)^2}{{d_p}^2\varepsilon^3}u_s + \frac{1.75\rho(1-\varepsilon)}{d_p\varepsilon^3}{u_s}^2 \quad (5)$$

where u_s is the superficial velocity, which can be calculated as:

$$u_s = \varepsilon.u_{Physical} \quad (6)$$

The viscous term becomes significant at low velocities, while the inertial term becomes essential at high velocities. According to the Ergun equation (Eq. 6), the viscous ($1/K$) and inertial ($C_{inertial}$) resistance coefficients are calculated as:

$$K = \frac{3.5(1-\varepsilon)}{\varepsilon^3.d_p} \quad (7)$$

$$C_{inertial} = \frac{\varepsilon^3.{d_p}^2}{150(1-\varepsilon)^2} \quad (8)$$

Concerning thermal volume-averaged models, there are two possibilities:

- Local Thermal Non-Equilibrium Model (LTNEM)
- Local Thermal Equilibrium Model (LTEM)

This study employs LTNEM to model temperature distribution in a porous rock bed, allowing for distinct solid (T_s) and fluid (T_f) temperature fields. This approach is essential when heat transfer between phases is slower than internal heat transport, creating significant temperature gradients. The model solves two coupled energy equations linked by an interfacial heat transfer term.

Energy conservation equation for the fluid region of the rock bed [7]:

$$C_{P,f}\frac{\partial T_f}{\partial t} + \boldsymbol{u}.\nabla T_f = \alpha_f\nabla^2 T_f + h_{fs}A_{fs}(T_s - T_f) \quad (9)$$

Energy conservation equation for the solid region of the rock bed [7]:

$$(1-\varepsilon)C_{P,s}\frac{\partial T_s}{\partial t} = (1-\varepsilon)\alpha_s\nabla^2 T_s + h_{fs}A_{fs}(T_f - T_s) \quad (10)$$

where C_P is the specific heat capacity. Indexes s and f belong to the solid and fluid sections, respectively. Also, k is the thermal conductivity. Moreover, h_{fs} is the heat transfer coefficient, which is defined as follows:

$$h_{fs} = \frac{\mathrm{k}_f}{d_p}Nu \quad (11)$$

where Nu is the fluid-solid Nusselt number, which is defined by a correlation presented by Wakao et al. [13] as follows:

$$Nu = \left[2 + 1.1Re^{0.6}Pr^{1/3}\right] \quad (12)$$

Furthermore, A_{fs} is the rock bed-specific area that is defined as:

$$A_{fs} = 6\frac{(1-\varepsilon)}{d_p} \quad (13)$$

The thermophysical properties of the employed materials, including the air and the magnetite [12], are listed in Table II.

TABLE II. THERMOPHYSICAL CHARECTERISTICS OF THE EMPLOYED MATERIALS IN THE SIMULATION

Property		Air	Magnetite
Density [kg.m^{-3}]	ρ	1.225	5170
Thermal Conductivity [W·m^{-1}·K^{-1}]	k	0.0242	5.1
Specific Heat Capacity [J·Kg^{-1}·K^{-1}]	C_p	1006.43	651.3
Dynamic Viscosity [Pa·s]	μ	1.7894×10^{-05}	-

The boundary conditions (BCs) used for the inlet and outlet of the computational domain are velocity_inlet and outflow. No slip BC is considered for the outer wall of the computational domain with adiabatic thermal BC. The initial and boundary conditions of the thermal field are the same as the experimental conditions listed in Table I. The simulation is conducted over 8 hours, encompassing two complete charge and discharge cycles, each lasting 2 hours. At the start of the simulation, the entire computational domain is initialized at 23°C. The input thermal BCs are set to 70°C for the charging phase and 31°C for the discharging phase. The details of the numerical solver are listed in Table III.

TABLE III. DETAILS OF THE NUMERICAL SOLVER

Pressure-Velocity Coupling	Coupled
Spatial Discretization	
Gradients	Least Squares Cell Based
Pressure	Second Order
Momentum	First Order Upwind
Turbulent Kinetic Energy	First Order Upwind
Specific Dissipation Rate	First Order Upwind
Energy	Second Order Upwind
Transient Formulation	First Order Implicit

A structured grid with 219,834 hexahedron cells is employed for the simulations. The maximum wall coordinate Y^+ is 50.69. In the present work, the employed *k-ω SST* turbulence model uses a blending function to transition from *k-ω* (near-wall) to *k-ε* (far from the wall), enabling wall functions

when needed. In this case, $30<Y^{+}<300$ is acceptable and leads to the use of mainly the *k-ε* closure. The time step for transient modeling was 1 second with 100 maximum iterations per time step for better convergence.

III. Results and Discussions

Repeatability analysis ensures consistency, minimizes errors and enhances reliability in experimental tests. It validates methods, strengthens reproducibility, and supports robust decision-making in research and industry by providing accurate, comparable, and high-quality results. The results of the repeatability analysis for the seven sensors in the present experimental setup were presented in our previous work [12]. However, for instance, the results of the repeatability analysis for sensor two are illustrated in Figure 2. Consequently, the maximum error for this sensor is 9.46%, which shows the reliability of the experimental outcomes.

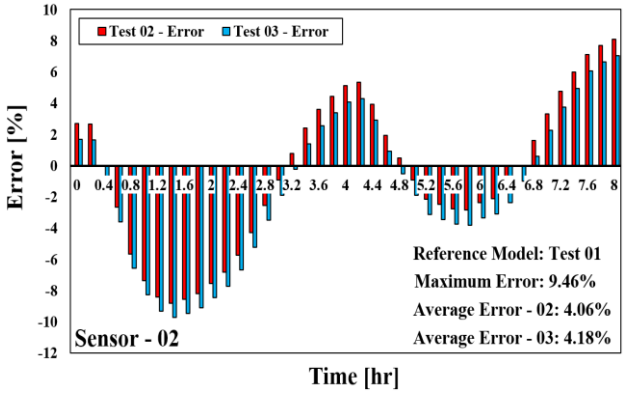

Figure 2. The results of the repeatability analysis of the experimental setup [12]

The experimental results of this work were published in our previous conference paper [12]; for instance, one of them is demonstrated in Figure 3. The experimental results are from two cycles of two-hour tests for both charging and discharging processes. Sensors 1 to 7 are inserted inside the porous media; however, sensors "*Wall 01*" to "*Wall 03*" were inserted on the rock bed's outer surface to ensure the setup's insulation.

Figure 4 illustrates an acceptable agreement between the numerical model and the experimental results. Accordingly, it can be seen that among these four sensors, the maximum error is 1.67%. The simulations were performed for all test periods. The results of validation analysis for the remaining sensors (5 to 7) are demonstrated in Figure 5.

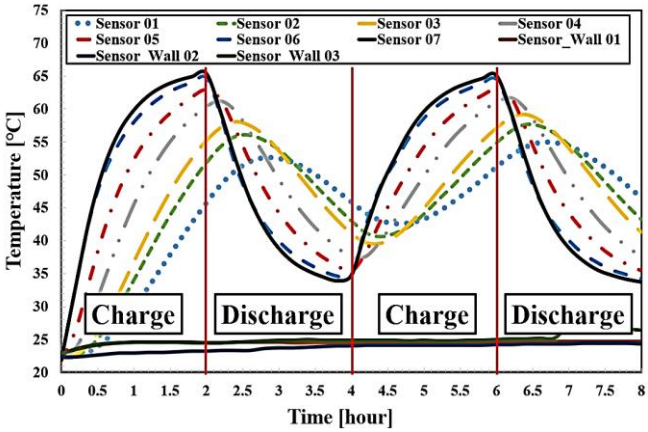

Figure 3. The experimental results for two cycles of two-hour tests for both charge and discharge [12]

The results of validation analysis for sensors 1 to 4 are demonstrated in Figure 4.

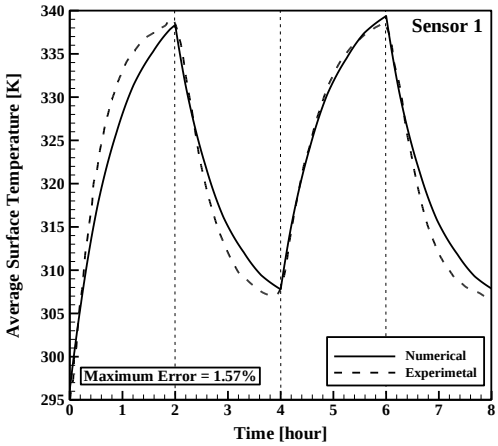

(a)

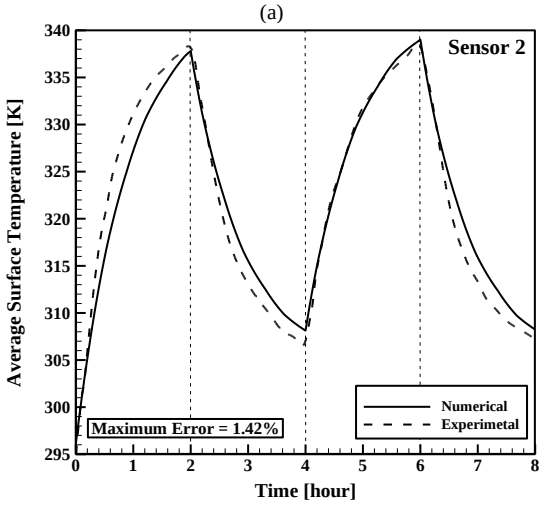

(b)

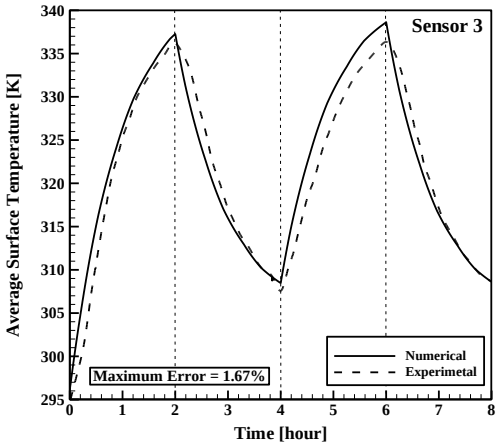

(c)

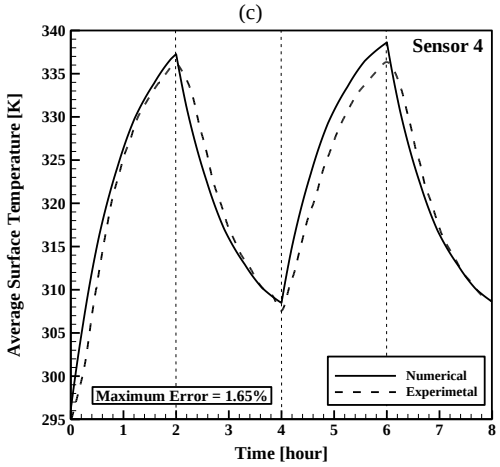

(d)

Figure 4. The results of validation analysis for (a) sensor 1, (b) sensor 2, (c) sensor 3, and (d) sensor 4

The main point that can be realized in the experimental results shown in Figures 3 and 5 is that, for sensors 5 to 7, which are inserted far from the inlet, the maximum and minimum temperatures are not achieved at the start or end of the process. In other words, when the charging process is stopped, and the discharge process starts, the recorded data show that the region continues the previous process. For instance, at 2 hours, the charging process is stopped, marking the start of the discharge process. However, it can be seen that sensors 5-7 are still in the mood of charging. The physical reason behind this phenomenon is that, although the inlet temperature changes from 70℃ to 31 ℃ (from charging to discharging modes), the heat is transferred from the early part of the rock bed to the regions of sensors 5-7.

The results of validation analysis for sensors 5 to 7 are presented in Figure 5. Accordingly, it can be seen that the maximum quantitative error for these sensors is 6%. Although the obtained quantitative error between the numerical and experimental outcomes for sensors 5-7 is acceptable, however, the numerical model could not accurately model the physical phenomenon occurring at the points related to sensors 5 to 7, which is due to the delay in heat transfer from the initial to the final points of the bed, which is one of the weaknesses of the proposed numerical model.

The 2D velocity magnitude contours at the X = 0 m slice are illustrated in Figure 6. At the inlet section, the velocity profile shows a developing flow pattern as the fluid enters the domain. The porous section in the middle introduces resistance, significantly reducing velocity and a more uniform flow distribution. The outlet section exhibits a stabilized velocity profile, indicating the transition to a fully developed flow. The porous region enforces a more diffused velocity field due to flow resistance.

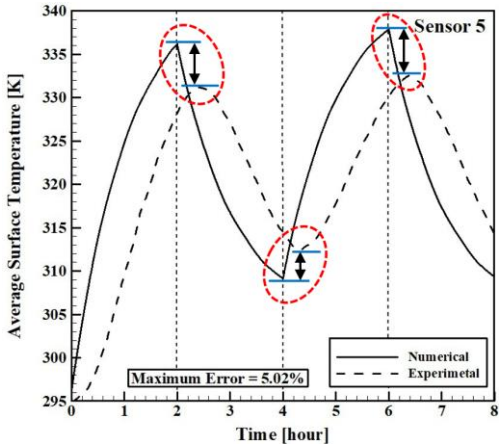

(a)

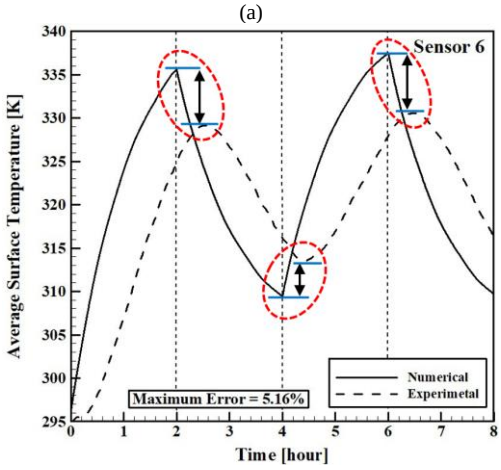

(b)

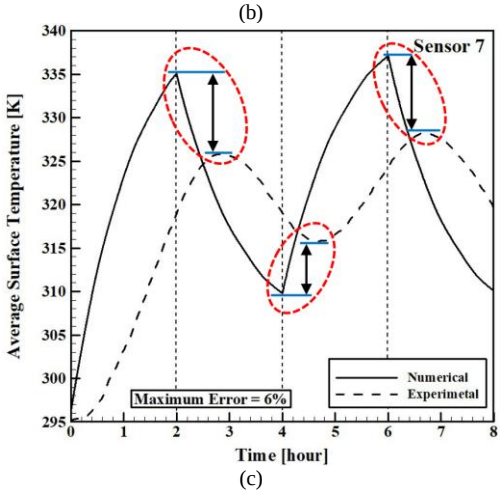

(c)

Figure 5. The results of validation analysis for (a) sensor 5, (b) sensor 6, and (c) sensor 7

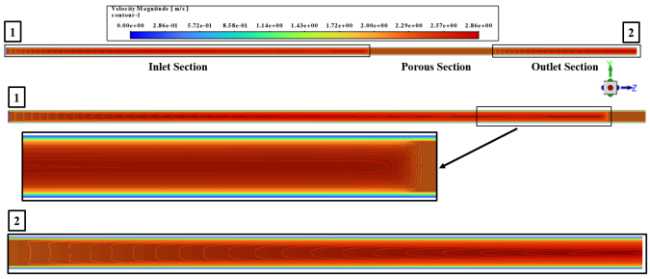

Figure 6. The 2D velocity magnitude contours at the slice of X = 0 m

The comparison of numerical outcomes for average surface temperature profiles in different locations (sensors) is presented in Figure 7. During each charge phase, the temperature increases, reaching T_{Max} values of 338.34 K and 339.39 K at approximately 2 and 6 hours, respectively. During the discharge phases, the temperature drops to T_{Min} values of 307.78 K and 307.86 K. The temperature differences (ΔT) between peak and trough points are also indicated, with ΔT values of 3.27 K for the first charge and 2.25 K for the second charge, while the discharge cycles show ΔT values of 2.01 K and 2.21 K, respectively. The figure shows high consistency across all sensors, confirming the numerical stability and validity of the temperature predictions. The small variations between cycles for different sensors (locations) illustrate the temperature distribution along the porous region (rock bed). This analysis highlights the thermal dynamics of the system, demonstrating cyclic temperature fluctuations and providing valuable insight into thermal behavior.SSS

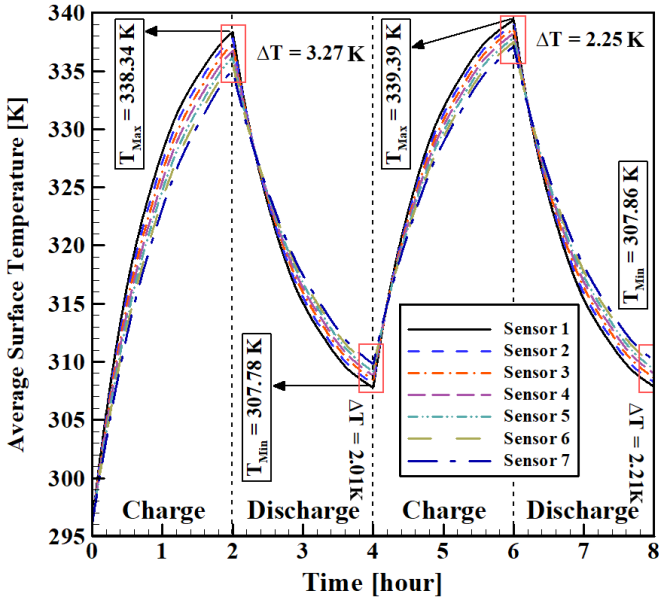

Figure 7. The comparison between the numerical outcomes of average surface temperature profiles in different locations

IV. Conclusion

In this study, LTNEM was employed to model heat transfer in a magnetite-based rock bed with a horizontal cylindrical design, capturing the distinct temperature fields of the solid and fluid phases. By experimentally analyzing charging and discharging processes and validating results through CFD simulations, the study demonstrated the accuracy of the developed LTNEM in predicting the thermal behavior of a porous rock bed. The findings highlight the importance of accounting for interfacial heat transfer in systems where thermal equilibrium assumptions may not be valid. A comparison between experimental and numerical outcomes showed a maximum error of 6%, validating the model's reliability for predicting heat transfer dynamics in the magnetite-based rock bed. Although the obtained maximum error falls within the acceptable range, the developed code could not accurately capture the temperature profile trend across the entire domain. This limitation will be addressed in future work.

References

[1] Sadeghi, G. (2022). Energy storage on demand: Thermal energy storage development, materials, design, and integration challenges. *Energy Storage Materials*, 46, 192-222.

[2] Fernández, A., Martínez, M., Segarra, M., Martorell, I., & Cabeza, L. F. (2010). Selection of materials with potential in sensible thermal energy storage. *Solar Energy Materials and Solar Cells*, 94(10), 1723-1729.

[3] Mousavi Ajarostaghi, S. S., Amiri, L., & Poncet, S. (2024). Application of Thermal Batteries in Greenhouses. *Applied Sciences*, 14(19), 8640.

[4] Dincer, I., & Rosen, M. A. (2011). *Thermal energy storage: systems and applications*. John Wiley & Sons.

[5] Fernández, A. I., Marti, J., & Cabeza, L. F. (2019). Review on thermal energy storage applications in concentrated solar power plants. *Renewable and Sustainable Energy Reviews*, 112, 253-271.

[6] Amiri, L., Ermagan, H., Kurnia, J. C., Hassani, F., & Sasmito, A. P. (2024). Progress on rock thermal energy storage (RTES): A state of the art review. *Energy Science & Engineering*, 12(2), 410-437.

[7] Nield, D. A., & Bejan, A. (2006). *Convection in porous media*, vol. 3, pp. 629-982. New York: Springer.

[8] Ergun, S. (1952). Fluid flow through packed columns. *Chemical Engineering Progress*, 48(2), 89.

[9] Parhizi, M., Torabi, M., & Jain, A. (2021). Local thermal non-equilibrium (LTNE) model for developed flow in porous media with spatially-varying Biot number. *International Journal of Heat and Mass Transfer*, 164, 120538.

[10] Liu, S., Ahmadi-Senichault, A., Levet, C., & Lachaud, J. (2024). Development and validation of a local thermal non-equilibrium model for high-temperature thermal energy storage in packed beds. *Journal of Energy Storage*, 78, 109957.

[11] Mousavi Ajarostaghi, S. S., Amiri, L., & Poncet, S. Sensible Heat Thermal Energy Storage as Thermal Battery; Experimental Evaluation of Low-Temperature Charge and Discharge Process in a Rock-Bed. *CSME/CFD Canada International Conference 2024*, May 26–29, 2024, University of Toronto, Ontario, Canada.

[12] Grosu, Y., Faik, A., Ortega-Fernández, I., & D'Aguanno, B. (2017). Natural Magnetite for thermal energy storage: Excellent thermophysical properties, reversible latent heat transition and controlled thermal conductivity. *Solar Energy Materials and Solar Cells*, 161, 170-176.

[13] Wakao, N., & Kagei, S. (1982). *Heat and mass transfer in packed beds* (Vol. 1). Taylor & Francis.